ADVANCED MATERIALS TECHNOLOGIES
www.advmattechnol.de

In-Flow MOF Lithography

*Semih Sevim, Carlos Franco, Hongjun Liu, Hervé Roussel, Laetitia Rapenne, Juan Rubio-Zuazo, Xiang-Zhong Chen, Salvador Pané, David Muñoz-Rojas, Andrew J. deMello, and Josep Puigmartí-Luis**

Continuous-flow microfluidic systems are widely recognized as advanced and robust tools for materials synthesis. Indeed, the exquisite spatiotemporal control over reagent concentrations in a microfluidic channel has enabled the formation of composite materials and structures with unique features. Herein, we show for the first time that by combining reactive substrates with continuous-flow microfluidic devices, material growth can be spatiotemporally driven and modulated on a surface. We demonstrate such unprecedented control by crystallizing and patterning compositional gradients of HKUST-1 (a widely investigated metal-organic framework (MOF)) on a reactive surface. We believe that this novel approach will engender new possibilities for incorporating MOFs on reactive surfaces, and thus for developing new advanced technological architectures and devices.

Surfaces play a key role in many aspects of nanotechnology, as they can control the orientation, localization, and integration of functional materials in advanced technological systems and devices.[1–5] However, the production of new marketable products based on nanotechnology developments will be efficiently accomplished when such control will be applied from the molecular level to the macroscale.[6–8] At the macroscale, functional materials can be efficiently interfaced (connected) to read-out components for device fabrication. Accordingly, the last two decades have seen a remarkable increase in the number of methods able to integrate functional materials on surfaces for micro- and nano-electromechanical systems applications. In this respect, methods based on atomic layer deposition (ALD) and chemical vapor deposition (CVD),[9,10] 3D printing,[11–13] and microfluidic technologies[14–16] have emerged as disruptive tools in such manufacturing environments.

Functional materials such as porous coordination polymers (also known as metal–organic frameworks or MOFs) have been the focus of much recent attention owing to their tunable physicochemical properties.[17–19] MOFs are constructed from metal ions (or clusters) and organic ligands, with their synthesis and growth typically being performed in solution. However, the bulk solution synthesis of MOFs does not facilitate their effective incorporation into devices, thus hampering their widespread application. Unsurprisingly, much current effort is focused on integrating MOF materials on surfaces by controlling their orientation and grain structure (e.g., compactness).[20–24] Certainly, by reaching this level of integration (i.e., crystal orientation and grain boundary), MOFs will have the potential to unleash their practical use in other research areas such as, for example, semiconductor devices.[25–28] To date, a range of different approaches for the integration of MOFs on surfaces have been investigated, including layer-by-layer deposition,[29,30] Langmuir–Blodgett deposition,[31,32] lithography,[33–35] CVD,[36] and seeded growth from both reactive metal templates[37–39] and self-assembled monolayers (SAMs).[40] Interestingly, studies addressing the nucleation and growth of MOFs on SAM-functionalized surfaces indicate that the functional end-groups present on the surface determine the crystallographic orientation of surface-grown MOFs.[41,42] However, while successful strategies have been demonstrated, current technologies cannot exert sufficient control over concentration gradients of metal ions and organic ligands (on the surface) during MOF growth. This lack of control hinders the formation of compositional MOF gradients on surfaces and limits the rational design of defects. Importantly, new approaches for an accurate control of MOF gradients (and MOF defect engineering) will dramatically increase the number of applications and functions of MOF films.[43,44] To this end, herein, we successfully develop

S. Sevim, Dr. C. Franco, Prof. A. J. deMello, Dr. J. Puigmartí-Luis
Institute of Chemical and Bioengineering
ETH Zurich
Vladimir Prelog Weg 1, 8093 Zurich, Switzerland
E-mail: josep.puigmarti@chem.ethz.ch
Dr. H. Liu, H. Roussel, L. Rapenne, Dr. D. Muñoz-Rojas
Institute of Engineering
Univ. Grenoble Alpes
CNRS
Grenoble INP
LMGP
F-38000 Grenoble, France
Dr. J. Rubio-Zuazo
Spanish CRG BM25-SpLine Beamline at the ESRF
71 Av des Martyrs CS 40220, 38043 Grenoble Cedex 9, France
Dr. J. Rubio-Zuazo
Instituto de Ciencia de Materiales de Madrid—ICMM/CSIC
Cantoblanco E-28049, Madrid, Spain
Dr. X.-Z. Chen, Dr. S. Pané
Multi-Scale Robotics Lab (MSRL)
Institute of Robotics and Intelligent Systems (IRIS)
ETH Zurich
Tannenstrasse 3, 8092 Zurich, Switzerland
The ORCID identification number(s) for the author(s) of this article can be found under https://doi.org/10.1002/admt.201800666.

DOI: 10.1002/admt.201800666

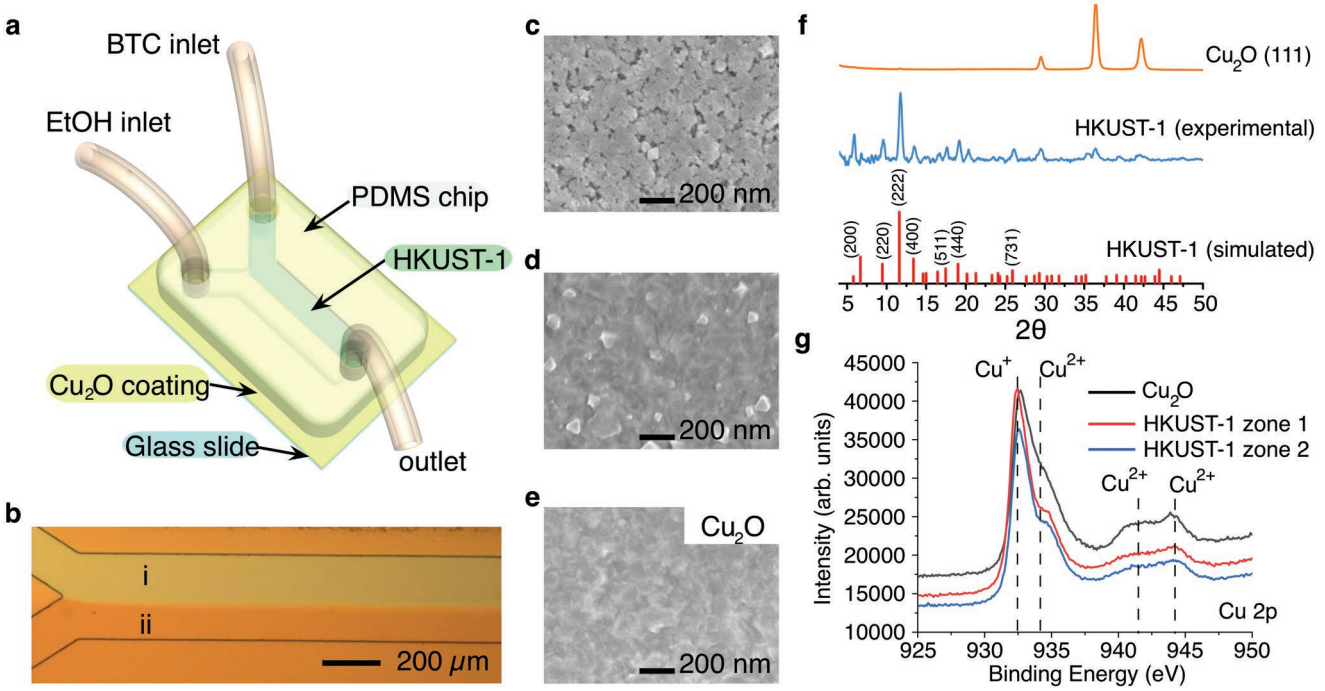

Figure 1. a) Schematic illustration of the Y-shaped microfluidic device used in our investigations. b) Optical image of the microfluidic channel during the growth of HKUST-1 in a coflow configuration between i) an H_3BTC-laden stream and ii) ethanol. It is noted that the bluish region is located where H_3BTC is injected, i.e., on the (i) side of the channel. c–e) SEM images of the bluish area ((i) area), Cu_2O inside the microfluidic channel ((ii) area), and Cu_2O outside the microfluidic device. f) Grazing Incidence X-ray Diffraction (GIXRD) spectra of Cu_2O (111), HKUST-1 generated inside the microfluidic channel, and the simulated XRD pattern of HKUST-1. g) XPS spectra of Cu_2O (111) and of material in the bluish area generated inside the microfluidic channel. In the latter, two different zones along the length of the microfluidic channel are measured for comparison.

a simple strategy to synthesize, pattern, and grow compositional gradients of a well-known MOF (Hong Kong University of Science and Technology (HKUST)-1) on reactive surfaces through the use of continuous flow microfluidics. HKUST-1 ($Cu_3(BTC)_2(H_2O)_3$, BTC = 1,3,5-benzenetricarboxylate) was used in the current study since it is a model MOF compound that has been extensively studied on surfaces[45–47] and can be easily synthesized under mild conditions[48,49] for different applications, i.e., gas separation,[50] catalysis,[51] and sensing.[25] Specifically, we integrate a highly textured Cu_2O (111) surface within a microfluidic device, in which an ethanolic solution of benzene-1,3,5-tricarboxylic acid (H_3BTC) is flowed. Because of the deprotonation of H_3BTC into BTC^{3-}, this solution is mildly acidic (with a pH of approximately 5) and partially dissolves the Cu^+ ions of the textured surface. Molecular oxygen present in the ethanol stream causes the oxidation of Cu^+ into Cu^{2+},[52] which is coordinated by BTC^{3-}, subsequently inducing the nucleation of HKUST-1. It should be noted that the microfluidic devices used throughout the current study are structured from polydimethylsiloxane (PDMS), a silicone-based elastomer that is highly permeable to gases such as molecular oxygen.

In a typical experiment, a Y-shaped microfluidic reactor consisting of two inlets and one outlet is used to synthesize HKUST-1 (**Figure 1**a). This configuration, in contrast to other reported methods, allows the direct formation of BTC^{3-} concentration gradients inside a microfluidic channel when the incorporation of an unreactive flow inside the microfluidic device is considered (vide infra). Initially, to clearly determine the effect of a reactive and unreactive flows, we injected a saturated ethanolic solution of H_3BTC (reactive flow) and pure ethanol (unreactive flow) at constant flow rate of 10 μL min^{-1} through the inlets (Figure 1a). As expected, we observed that the two solutions coflow in a side-by-side arrangement within the main microfluidic channel due to the low associated Reynolds number that was calculated to be below 2 (Figure 1b).[53,54] After 3 h of constant operation, a distinct color change (from orange to blue) of the surface below the stream containing H_3BTC could be observed (Figure 1b). This color change is attributed to the formation of HKUST-1 on the Cu_2O substrate (Figure 1b, **Figure 2**, and Movie S1, Supporting Information). Additionally, we examined the reacted ((i) in Figure 1b) and unreacted ((ii) in Figure 1b) regions of the microfluidic channel using scanning electron microscopy (SEM) after device disassembly. SEM images reveal that the bluish area is formed as a compact film that perfectly covers the entire length of the microfluidic channel (Figure 1c). This film comprises particles with a smooth and dense appearance. In contrast, the surface exposed to the pure ethanol stream contains few particles (Figure 1d), those of which are probably formed by diffusion of H_3BTC into the ethanol stream. Outside the microfluidic channel, the Cu_2O (111) surface was smooth and contained no particles (Figure 1e).

Subsequently, X-ray diffraction (XRD) and X-ray photoelectron spectroscopy (XPS) analysis were used to confirm the formation of HKUST-1 inside the microfluidic channel. X-ray patterns were obtained via grazing incidence diffraction

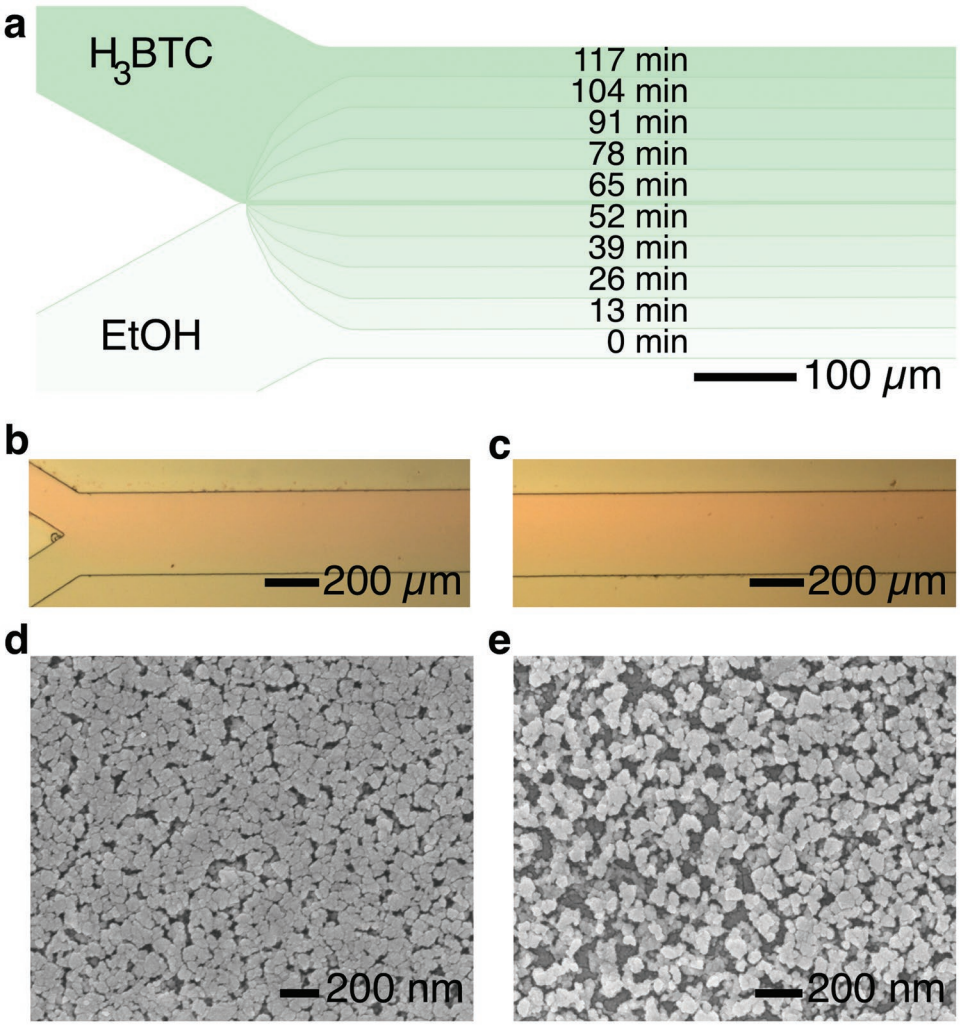

Figure 2. a) Schematic illustration of the generation of graded HKUST-1 surfaces inside the microfluidic channel. The time scale represents the total exposure time of the surface to the H_3BTC stream. This controlled exposure can be accomplished by varying the flow rate of H_3BTC (reactive) and ethanol (unreactive) flows. b,c) Optical images of the microfluidic channel after the formation of the graded HKUST-1 film at the inlet and outlet of the microfluidic channel, respectively. (d) and (e) are SEM images taken across the width of the microfluidic channel where the graded surface has been generated. The image shown in (d) was acquired in the region where the H_3BTC stream was allowed to flow for more than 100 min, whereas the image shown in (e) was acquired in the region where the H_3BTC stream was allowed to flow for 60 min.

experiments involving two incidence angles (see the Experimental Section for further details). As shown in Figure 1f, at an incidence angle of 0.1° the reflections corresponding to HKUST-1 were clearly observed, along with some reflections from Cu_2O (111). The calculated XRD spectra of HKUST-1 are shown in Figure 1f for comparison. In contrast, at an incidence angle of 0.35°, the Cu_2O (111) reflections were far more pronounced vanishing completely the HKUST-1 reflections (Figure S1, Supporting Information). We also tried to grow HKUST-1 from a Cu_2O substrate of different texture, i.e., Cu_2O (110). Grazing incidence X-ray diffraction (GIXRD) spectra showing reflections for HKUST-1 grown on both Cu_2O (110) and Cu_2O (111) surfaces are shown in Figure S2 in the Supporting Information. The clear variations in peak intensities between the two Cu_2O textures could indicate a possible role of surface crystallographic orientation on HKUST-1 growth. To confirm this hypothesis, we conducted transmission electron microscopy (TEM) analyses on cross-sectioned samples. The resulting TEM images (Figure S3a, Supporting Information) clearly show the presence of a 15 nm thick layer on top of the Cu_2O film that we attribute to the HKUST-1 film (see also Figure S4, Supporting Information). Unfortunately, selected area electron diffraction patterns of this layer only indicated the presence of metallic copper nanoparticles (Figure S3b, Supporting Information). Accordingly, we assume that the electron beam reduces the copper ions within the HKUST-1 film,[55] preventing an evaluation of epitaxy in our samples.

Figure 1g shows the XPS spectra (Cu 2p edge) of the Cu_2O film (outside the microfluidic channel) as well as the XPS spectra of two areas inside the microfluidic channel. While the XPS spectrum of Cu_2O (111) shows a typical asymmetric peak at 933 eV, with satellite signals between 940 and 945 eV,[56] the XPS spectrum measured inside the microfluidic channel exhibits a clear elbow in the Cu 2p3/2 signal that corresponds to Cu^{2+}.[57]

Accordingly, and despite the fact that the HKUST-1 film is on top of the Cu_2O (111) film, a clear increase in the amount of Cu^{2+} is observed from ≈40% to ≈60% (see Figure S5, Supporting Information). Thus, we can conclude that a localized growth of HKUST-1 films on a surface can be accomplished in flow.

Strikingly, under the same experimental conditions (i.e., fixed H_3BTC concentration, temperature, and reaction time) compact HKUST-1 films could not be grown in a beaker where confinement during the reactive process was missing (see the Experimental Section for further details and Figure S6, Supporting Information).[58] In this situation, only isolated and polydisperse HKUST-1 crystals were observed on the Cu_2O (111) substrate. Accordingly, these results clearly indicate that mass transport is crucial for the controlled growth of a compact and homogeneous HKUST-1 film.

To demonstrate the versatility of our approach, we took advantage of the controlled molecular diffusion of reagent-laden flows in Y-shaped microfluidic devices to design compositionally graded HKUST-1 surfaces. To this end, the flow rate of the H_3BTC solution (FR_{H3BTC}) was progressively increased while the flow rate of pure ethanol (FR_{EtOH}) was decreased (Figure 2a). In these experiments, the total flow rate ($FR_{EtOH} + FR_{H3BTC}$) was maintained at 20 μL min^{-1} (see the Experimental Section for details). As shown in Figure 2b,c, controlled chemical oxidation and coordination on the surface led to a compositionally graded film within the microfluidic channel. This was confirmed by assessing SEM images across the width of the microfluidic channel, where we observed different levels of compactness in the region where HKUST-1 was grown (e.g., Figure 2d,e). As expected, the compactness of the HKUST-1 film decreased toward the side of the microfluidic channel where the pure ethanol stream was located (Figure 2e).

Next, we conducted experiments in which different H_3BTC flow configurations were used to localize the formation of HKUST-1 films and generate complex 2D patterns of any shape on reactive Cu_2O (111) surfaces. For example, we patterned serpentine structures (**Figure 3**b) and other geometrically challenging forms with high accuracy (Figure 3d). Moreover, our approach allows for the simultaneous formation of multiple patterns inside a microfluidic channel when the number of coflowing streams is increased. An example of such a scenario is illustrated in Figure 3e,f and Movie S2 in the Supporting Information, in which two parallel HKUST-1 patterns are obtained by alternating four coflowing streams (two of pure ethanol and two of an H_3BTC solution). Importantly, SEM characterization of material within the bluish region indicates, again, the formation of a compact HKUST-1 film with a dense and smooth appearance, whereas the orange patterned regions only contain a small number of diminutive crystals that are formed as a consequence of diffusion of H_3BTC into the ethanol streams (Figure 3g,h, respectively).

In summary, we have shown a novel strategy for the growth and integration of intricate MOF architectures on highly oriented copper oxide surfaces using continuous-flow microfluidics. Furthermore, we have shown that the ability to precisely control reagent diffusion inside confined environments is key to achieving homogeneous and compact MOF films. In the current experiments, our approach is successful in creating highly packed HKUST-1 films under mild conditions (i.e., room temperature and pressure) as well as forming compositional gradients of HKUST-1. Accordingly, we believe that our technology has the potential to open new horizons in the controlled fabrication of compositional and structural MOF architectures on surfaces, which will engender a range of novel MOF-based devices.

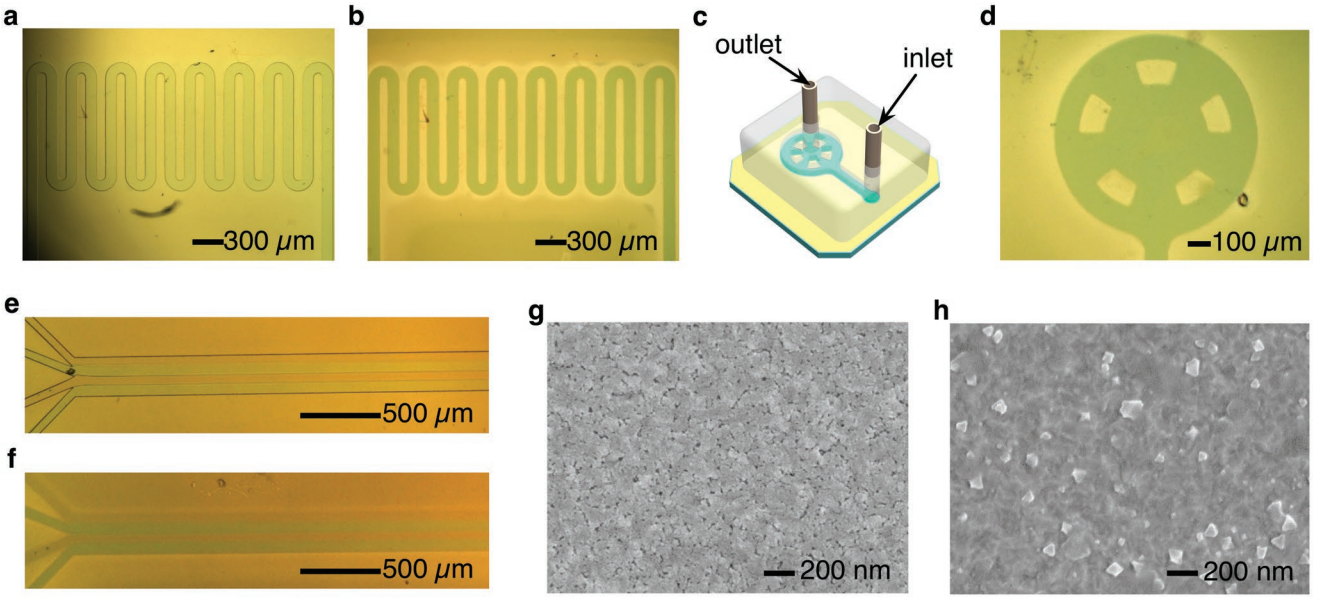

Figure 3. Images acquired a) during and b) after the synthesis of HKUST-1 inside a serpentine microfluidic channel. In (b), the PDMS slab containing the microfluidic channel has been removed from the surface. c) Schematic illustration of a microfluidic channel with a wagon wheel shape showing inlet and outlet positions. d) Image of a patterned HKUST-1 film taken after removing the PDMS slab containing the microfluidic channel with a wagon wheel shape. e,f) Images illustrating the parallel synthesis of HKUST-1 using multiple coflowing streams. In (f) the PDMS slab has been removed from the patterned surface. (g) and (h) present SEM images of the bluish area and the orange regions located inside the microfluidic channel after synthesis.

Experimental Section

Materials: PDMS base and curing agent were purchased as a Sylgard 184 Silicone elastomer kit from Dow Europe, Wiesbaden, Germany. Benzene-1,3,5-tricarboxylic acid (H_3BTC) was obtained from Sigma-Aldrich (St. Louis, USA). High performance liquid chromatography (HPLC) grade ethanol was purchased from VWR International (Fontenay-sous-Bois, France).

Cu_2O Coated Glass Surfaces:[59] Cu_2O films were deposited via Aerosol Assisted metal-organic chemical vapor deposition (MOCVD) using a homemade system. A 0.01 M trifluoroacetylacetonate (Strem Chemicals, Newburyport, Massachusetts, USA) solution in 0.5 L of absolute ethanol (Sigma-Aldrich, 99%, St. Louis, USA) was prepared. This precursor solution was atomized into fine droplets by a piezoelectric ceramic at 4.2 Hz and 6 W, forming a mist on top of the solution. The mist was then transported by a flow of nitrogen (2 L min^{-1}) into the deposition chamber (consuming the solution at a rate of 1.5 mL min^{-1}). The oxidizing gas flow was obtained by mixing 3 L min^{-1} flow of N_2 with a 5 L min^{-1} flow of air (12% of O_2). The oxidizing flow was divided in two separate lines: one that was bubbled through water at room temperature, to maintain humidity during the deposition process, and a second that was fed directly to the reactor. The humidity of the carrier gas could then be controlled by adjusting the relative flow rates. The deposition chamber was maintained at close to atmospheric pressure, with deposition being performed at 335 °C onto planar glass substrates (Carl Roth, Karlsruhe, Germany).

Microfluidic Device Fabrication: The silicon master molds used in the fabrication of microfluidic devices were fabricated using standard photolithography techniques.[60] Subsequently, a replica molding workflow was used to produce the microfluidic devices themselves. First, the silicon master mold was passivated with chlorotrimethylsilane under vacuum for 30 min. Then a mixture of PDMS base and curing agent (Sylgard 184 Silicone elastomer kit) mixed in a 10:1 ratio by weight was cast against the mold and cured at 70 °C overnight. The cured PDMS was peeled-off the master mold and diced using a razor blade. The inlets and the outlet were formed using a 1.5 mm biopsy punch (1.5 mm, Miltex GmBH, Rietheim-Weilheim, Germany). All channels in the Y-shaped microfluidic device had a height of 50 µm, with the main channel having a width of 300 µm. In addition, the serpentine microfluidic device integrated a channel with a height and width of 30 and 100 µm, respectively. Features in the four-inlet microfluidic device were 50 µm high, with the width of the main channel being 250 µm.

Videos/Optical Images: Videos and optical images were taken using a Nikon Eclipse Ti microscope (Amsterdam, Netherlands) equipped with a RETIGA R1 color camera (Rochester, USA).

Scanning Electron Microscopy: The SEM studies were performed on a Zeiss Ultra 55 microscope operating at an accelerating voltage of 5 kV. Samples were coated with a 4 nm thick film consisting of a mixture of Pt/Pd using a sputter Quorum Q150T-S.

Grazing Incidence X-Ray: GIXRD spectra were collected with a RIGAKU Smartlab (Neu-Isenburg, Germany) equipped with a 9 kW rotating anode Cu source (45 kV and 200 mA). A 1D parabolic mirror (with a divergence less than 0.05° in the 2θ direction), 2.5° Soller slits, a mask of 5.0 mm, and a 0.05 mm slit were positioned before the sample. The X-ray beam obtained was parallel to the sample surface. Optics after the sample included a 0.5 divergence thin film collimator, 2.5° Soller slits, no attenuator, and a punctual scintillator detector. A detector scan was performed between 2° and 80° (in 2θ scale) with steps of 0.04° and 2.4 s at each step. The omega incidence was 0.1° or 0.35°. During acquisition, the sample was kept in a horizontal orientation and held with double face Scotch tape.

Transmission Electron Microscopy: TEM observations were carried out at 200 kV with a JEOL 2010 microscope (resolution of 0.19 nm). Cross-section samples were prepared as thin wedge-shapes via automatized tripod polishing using a MultiPrep system (Allied High Tech Products, Inc., Campton, USA) and plastic diamond lapping films with grains of decreasing size (i.e., 15, 6, 3, 1, and 0.5 µm). The final polish was performed on a soft felt covered disc impregnated with a silica solution. Additionally, Ar ion milling was used during 2–5 min to minimize further the thickness.

X-Ray Photoelectron Spectroscopy: XPS analyses were carried out in a K-Alpha apparatus from Thermo Fisher Scientific (Zurich, Switzerland). In a UHV chamber (at 10^{-9} mbar), sample surfaces were irradiated with AlK_a radiation (1486.6 eV). Ejected electrons were collected by a hemispherical analyzer at 30 eV constant pass energy. The energy scale was calibrated with the C1s line from contamination carbon at 285.0 eV. Analyses were carried out at constant angle of 90° between the sample surface and the analyzer.

Microfluidic Synthesis of HKUST-1 on Cu_2O Surfaces: Prior to experiments, all microfluidics devices were clamped mechanically using a homemade stainless steel clamp over the Cu_2O coated glass slides. The H_3BTC saturated solution was prepared by dissolving 0.7 g of H_3BTC in 10 mL of ethanol, followed by heating and sonicating until a clear solution was obtained. Finally, the mixture was filtered using 0.45 µm Teflon syringe filters (Merck KGaA, Darmstadt, Germany).

Microfluidic Synthesis of HKUST-1 on Cu_2O Surfaces—Y-Shaped Microfluidic Chip (Isocratic Mode): A saturated solution of H_3BTC was pumped at 10 µL min^{-1} through one inlet, while EtOH was driven at the same flow rate via the other inlet. Cu_2O was exposed to both solutions over a period of 3 h. Finally, the surface was rinsed with EtOH (20 µL min^{-1}) for 3 min to eliminate excess H_3BTC solution.

Microfluidic Synthesis of HKUST-1 on Cu_2O Surfaces—Y-Shaped Microfluidic Chip (Gradient Mode): The microfluidic configuration employed was the same as for the isocratic mode. However, the relative flow rate (H_3BTC/EtOH) was now increased from 1:9 to 9:1 in nine steps, keeping the total flow rate at 20 µL min^{-1} (i.e., 2:18, 4:16,...,10:10,...16:4, 18:2 µL min^{-1}). Each step was performed for 13 min before changing the relative flow rate. Finally, the microchannel was washed with EtOH (at 20 µL min^{-1}) for 3 min.

Microfluidic Synthesis of HKUST-1 on Cu_2O Surfaces—Serpentine Microfluidic Chip and Wagon Wheel Shape: A solution of H_3BTC was injected into the microfluidic device at a constant flow rate of 10 µL min^{-1} for 2 h. The microchannel was then washed with EtOH (at 10 µL min^{-1}) for 3 min.

Microfluidic Synthesis of HKUST-1 on Cu_2O Surfaces—Four-Inlet Microfluidic Chip: Pure EtOH was injected into the first and third inlet, while H_3BTC was pumped through the second and fourth inlets. The flow rate in the four inlets was maintained at 15 µL min^{-1} for a period of 2 h. Finally, all the channels were rinsed with EtOH (at 10 µL min^{-1}) for 3 min.

Microfluidic Synthesis of HKUST-1 on Cu_2O Surfaces—Bulk Synthesis: A coated Cu_2O (111) glass slide was completely immersed in a beaker containing a saturated solution of H_3BTC for a period of 3 h and at room temperature. Reacted surfaces were then removed from the beaker and rinsed with copious amounts of EtOH.

Supporting Information

Supporting Information is available from the Wiley Online Library or from the author.

Acknowledgements

S.S. and C.F. contributed equally to this work. This work was supported by the European Union (ERC-2015-STG microCrysFact 677020) and the Swiss National Science Foundation (Project No. 200021_160174). J.P.-L. and D.M.-R. also acknowledge support from the European Union's Horizon 2020 FETOPEN-1-2016-2017 research and innovation program under grant agreement 801464. S.P. acknowledges financial support from a Consolidator Grant granted by the European Research Council (ERC) under the European Union's Horizon 2020 research and innovation program under Grant Agreement No. 771565. H.L. acknowledges the Ministère de l'Education nationale, de l'Enseignement supérieur et de la Recherche in France for a Ph.D. grant. D.M.-R. acknowledges funding through the Marie Curie Actions (FP7/2007-2013, Grant Agreement No. 63111). H.L. and D.M.-R. acknowledge the facilities, and the scientific and technical assistance of the CMTC characterization platform of

Grenoble INP (Institute of Engineering) supported by the Centre of Excellence of Multifunctional Architectured Materials "CEMAM" n°ANR-10-LABX-44-01 funded by the "Investments for the Future" Program. The authors thank Grégory Berthomé for the acquisition of the XPS spectra.

Conflict of Interest

The authors declare no conflict of interest.

Keywords

concentration gradient, metal–organic framework, microfluidics, MOF gradient, printing

Received: December 1, 2018
Revised: January 22, 2019
Published online:

[1] S. Marre, K. F. Jensen, *Chem. Soc. Rev.* **2010**, *39*, 1183.
[2] J. Puigmartí-Luis, D. Schaffhauser, B. R. Burg, P. S. Dittrich, *Adv. Mater.* **2010**, *22*, 2255.
[3] A. P. Alivisatos, *Science* **1996**, *271*, 933.
[4] M. Law, L. E. Greene, J. C. Johnson, R. Saykally, P. Yang, *Nat. Mater.* **2005**, *4*, 455.
[5] J. Li, L. Xu, T. Wang, J. Song, J. Chen, J. Xue, Y. Dong, B. Cai, Q. Shan, B. Han, H. Zeng, *Adv. Mater.* **2017**, *29*, 1603885.
[6] H. Song, M. A. Reed, T. Lee, *Adv. Mater.* **2011**, *23*, 1583.
[7] J. C. Love, L. A. Estroff, J. K. Kriebel, R. G. Nuzzo, G. M. Whitesides, *Chem. Rev.* **2005**, *105*, 1103.
[8] M. A. Boles, D. Ling, T. Hyeon, D. V. Talapin, *Nat. Mater.* **2016**, *15*, 141.
[9] X. Li, W. Cai, J. An, S. Kim, J. Nah, D. Yang, R. Piner, A. Velamakanni, I. Jung, E. Tutuc, S. K. Banerjee, L. Colombo, R. S. Ruoff, *Science* **2009**, *324*, 1312.
[10] A. M. van der Zande, P. Y. Huang, D. A. Chenet, T. C. Berkelbach, Y. You, G.-H. Lee, T. F. Heinz, D. R. Reichman, D. A. Muller, J. C. Hone, *Nat. Mater.* **2013**, *12*, 554.
[11] Y. L. Kong, I. A. Tamargo, H. Kim, B. N. Johnson, M. K. Gupta, T.-W. Koh, H.-A. Chin, D. A. Steingart, B. P. Rand, M. C. McAlpine, *Nano Lett.* **2014**, *14*, 7017.
[12] R. L. Truby, J. A. Lewis, *Nature* **2016**, *540*, 371.
[13] D. Kokkinis, M. Schaffner, A. R. Studart, *Nat. Commun.* **2015**, *6*, 8643.
[14] D. Therriault, S. R. White, J. A. Lewis, *Nat. Mater.* **2003**, *2*, 265.
[15] S. E. Chung, W. Park, S. Shin, S. A. Lee, S. Kwon, *Nat. Mater.* **2008**, *7*, 581.
[16] D. Rodríguez-San-Miguel, A. Abrishamkar, J. A. Navarro, R. Rodriguez-Trujillo, D. B. Amabilino, R. Mas-Ballesté, F. Zamora, J. Puigmartí-Luis, *Chem. Commun.* **2016**, *52*, 9212.
[17] O. M. Yaghi, M. O'Keeffe, N. W. Ockwig, H. K. Chae, M. Eddaoudi, J. Kim, *Nature* **2003**, *423*, 705.
[18] T. R. Cook, Y.-R. Zheng, P. J. Stang, *Chem. Rev.* **2013**, *113*, 734.
[19] I. Nath, J. Chakraborty, F. Verpoort, *Chem. Soc. Rev.* **2016**, *45*, 4127.
[20] P. Horcajada, C. Serre, D. Grosso, C. Boissière, S. Perruchas, C. Sanchez, G. Férey, *Adv. Mater.* **2009**, *21*, 1931.
[21] R. Ameloot, L. Stappers, J. Fransaer, L. Alaerts, B. F. Sels, D. E. De Vos, *Chem. Mater.* **2009**, *21*, 2580.
[22] A. Bétard, R. A. Fischer, *Chem. Rev.* **2012**, *112*, 1055.
[23] J.-L. Zhuang, A. Terfort, C. Wöll, *Coord. Chem. Rev.* **2016**, *307*, 391.
[24] P. Falcaro, K. Okada, T. Hara, K. Ikigaki, Y. Tokudome, A. W. Thornton, A. J. Hill, T. Williams, C. Doonan, M. Takahashi, *Nat. Mater.* **2017**, *16*, 342.
[25] A. A. Talin, A. Centrone, A. C. Ford, M. E. Foster, V. Stavila, P. Haney, R. A. Kinney, V. Szalai, F. E. Gabaly, H. P. Yoon, F. Léonard, M. D. Allendorf, *Science* **2014**, *343*, 66.
[26] L. Sun, M. G. Campbell, M. Dincă, *Angew. Chem., Int. Ed.* **2016**, *55*, 3566.
[27] D. Sheberla, J. C. Bachman, J. S. Elias, C.-J. Sun, Y. Shao-Horn, M. Dincă, *Nat. Mater.* **2017**, *16*, 220.
[28] P. Ramaswamy, N. E. Wong, G. K. H. Shimizu, *Chem. Soc. Rev.* **2014**, *43*, 5913.
[29] D. Zacher, O. Shekhah, C. Wöll, R. A. Fischer, *Chem. Soc. Rev.* **2009**, *38*, 1418.
[30] O. Shekhah, H. Wang, D. Zacher, R. A. Fischer, C. Wöll, *Angew. Chem., Int. Ed.* **2009**, *48*, 5038.
[31] R. Makiura, S. Motoyama, Y. Umemura, H. Yamanaka, O. Sakata, H. Kitagawa, *Nat. Mater.* **2010**, *9*, 565.
[32] S. Motoyama, R. Makiura, O. Sakata, H. Kitagawa, *J. Am. Chem. Soc.* **2011**, *133*, 5640.
[33] C. M. Doherty, G. Grenci, R. Riccò, J. I. Mardel, J. Reboul, S. Furukawa, S. Kitagawa, A. J. Hill, P. Falcaro, *Adv. Mater.* **2013**, *25*, 4701.
[34] P. Falcaro, R. Ricco, C. M. Doherty, K. Liang, A. J. Hill, M. J. Styles, *Chem. Soc. Rev.* **2014**, *43*, 5513.
[35] B. K. Keitz, C. J. Yu, J. R. Long, R. Ameloot, *Angew. Chem., Int. Ed.* **2014**, *53*, 5561.
[36] I. Stassen, M. Styles, G. Grenci, H. V. Gorp, W. Vanderlinden, S. D. Feyter, P. Falcaro, D. D. Vos, P. Vereecken, R. Ameloot, *Nat. Mater.* **2016**, *15*, 304.
[37] J. Reboul, S. Furukawa, N. Horike, M. Tsotsalas, K. Hirai, H. Uehara, M. Kondo, N. Louvain, O. Sakata, S. Kitagawa, *Nat. Mater.* **2012**, *11*, 717.
[38] K. Okada, R. Ricco, Y. Tokudome, M. J. Styles, A. J. Hill, M. Takahashi, P. Falcaro, *Adv. Funct. Mater.* **2014**, *24*, 1969.
[39] H. Ji, S. Hwang, K. Kim, C. Kim, N. C. Jeong, *ACS Appl. Mater. Interfaces* **2016**, *8*, 32414.
[40] S. Hermes, F. Schröder, R. Chelmowski, C. Wöll, R. A. Fischer, *J. Am. Chem. Soc.* **2005**, *127*, 13744.
[41] C. Munuera, O. Shekhah, H. Wang, C. Wöll, C. Ocal, *Phys. Chem. Chem. Phys.* **2008**, *10*, 7257.
[42] J.-L. Zhuang, M. Kind, C. M. Grytz, F. Farr, M. Diefenbach, S. Tussupbayev, M. C. Holthausen, A. Terfort, *J. Am. Chem. Soc.* **2015**, *137*, 8237.
[43] Z. Fang, B. Bueken, D. E. De Vos, R. A. Fischer, *Angew. Chem., Int. Ed.* **2015**, *54*, 7234.
[44] L. Yuan, M. Tian, J. Lan, X. Cao, X. Wang, Z. Chai, J. K. Gibson, W. Shi, *Chem. Commun.* **2018**, *54*, 370.
[45] E. Biemmi, C. Scherb, T. Bein, *J. Am. Chem. Soc.* **2007**, *129*, 8054.
[46] M. L. Ohnsorg, C. K. Beaudoin, M. E. Anderson, *Langmuir* **2015**, *31*, 6114.
[47] A. Summerfield, I. Cebula, M. Schröder, P. H. Beton, *J. Phys. Chem. C* **2015**, *119*, 23544.
[48] V. Stavila, J. Volponi, A. M. Katzenmeyer, M. C. Dixon, M. D. Allendorf, *Chem. Sci.* **2012**, *3*, 1531.
[49] J.-L. Zhuang, D. Ceglarek, S. Pethuraj, A. Terfort, *Adv. Funct. Mater.* **2011**, *21*, 1442.
[50] Y. Mao, J. Li, W. Cao, Y. Ying, L. Sun, X. Peng, *ACS Appl. Mater. Interfaces* **2014**, *6*, 4473.
[51] Y. Mao, J. Li, W. Cao, Y. Ying, P. Hu, Y. Liu, L. Sun, H. Wang, C. Jin, X. Peng, *Nat. Commun.* **2014**, *5*, 5532.
[52] G. Zhan, L. Fan, S. Zhou, X. Yang, *ACS Appl. Mater. Interfaces* **2018**, *10*, 35234.

[53] T. M. Squires, S. R. Quake, *Rev. Mod. Phys.* **2005**, *77*, 977.
[54] K. S. Elvira, X. C. i Solvas, R. C. R. Wootton, A. J. deMello, *Nat. Chem.* **2013**, *5*, 905.
[55] N. J. Long, A. K. Petford-Long, *Ultramicroscopy* **1986**, *20*, 151.
[56] J. A. Resende, *PhD Thesis*, Université Grenoble Alpes **2017**.
[57] Y. Wang, Y. Lü, W. Zhan, Z. Xie, Q. Kuang, L. Zheng, *J. Mater. Chem. A* **2015**, *3*, 12796.
[58] Note that we did not use any stirring during our batch experiments because this will result in turbulence mixing (affecting the mass transport in an uncontrolled way), and thus, this condition will not be comparable to the controlled diffusion-based mixing accomplished in the microfluidic experiments.
[59] H. Liu, V. H. Nguyen, H. Roussel, I. Gélard, L. Rapenne, J.-L. Deschanvres, C. Jiménez, D. Muñoz-Rojas, *Adv. Mater. Interfaces* **2018**, 1801364, https://doi.org/10.1002/admi.201801364.
[60] A. Abrishamkar, M. Paradinas, E. Bailo, R. Rodriguez-Trujillo, R. Pfattner, R. M. Rossi, C. Ocal, A. J. deMello, D. B. Amabilino, J. Puigmartí-Luis, *J. Visualized Exp.* **2016**, *113*, e54193.